

Characteristic radii of the Milky Way Globular Clusters

Andrés E. Piatti^{1,2*}, Jeremy Webb³ and Raymond Carlberg³

¹*Consejo Nacional de Investigaciones Científicas y Técnicas, Godoy Cruz 2290, C1425FQB, Buenos Aires, Argentina*

²*Observatorio Astronómico de Córdoba, Laprida 854, 5000, Córdoba, Argentina*

³*Department of Astronomy and Astrophysics, University of Toronto, 50 St. George Street, Toronto, ON, M5S 3H4, Canada*

Accepted XXX. Received YYY; in original form ZZZ

ABSTRACT

We report on the extent of the effects of the Milky Way’s gravitational field in shaping the structural parameters and internal dynamics of its globular cluster population. We make use of a homogeneous, up-to-date data set with kinematics, structural properties, current and initial masses of 156 globular clusters. In general, cluster radii increase as the Milky Way potential weakens; with the core and Jacobi radii being those which increase at the slowest and fastest rate respectively. We interpret this result as the innermost regions of globular clusters being less sensitive to changes in the tidal forces with the Galactocentric distance. The Milky Way’s gravitational field also seems to have differentially accelerated the internal dynamical evolution of individual clusters, with those toward the bulge appearing dynamically older. Finally we find a sub-population consisting of both compact and extended globular clusters (as defined by their r_h/r_J ratio) beyond 8 kpc that appear to have lost a large fraction of their initial mass lost via disruption. Moreover, we identify a third group with $r_h/r_J > 0.4$, which have lost an even larger fraction of their initial mass by disruption. In both cases the high fraction of mass lost is likely due to their large orbital eccentricities and inclination angles, which lead to them experiencing more tidal shocks at perigalacticon and during disc crossings. Comparing the structural and orbital parameters of individual clusters allows for constraints to be placed on whether or not their evolution was relaxation or tidally dominated.

Key words: Galaxy: globular clusters: general – Galaxy: structure – Galaxy: kinematics and dynamics

1 INTRODUCTION

It is widely accepted that Milky Way globular clusters have lost most of their masses through three main processes, namely: stellar evolution, two-body relaxation and tidal heating caused by the Milky Way’s gravitational field (Gnedin et al. 1999; Fall & Zhang 2001; Gieles & Baumgardt 2008; Webb et al. 2013, 2014; Brockamp et al. 2014; Alessandrini et al. 2014). Stellar evolution is most important during the first few hundred million years, while two-body relaxation becomes important as the mass loss rate due to stellar evolution continues to decrease (Hénon 1961; Gieles et al. 2011; Heggie & Hut 2003; Shukirgaliyev et al. 2018). Whether or not a cluster is strongly affected by the tidal field depends on its size, mass, and orbit within the Galaxy. Since the strength of the Milky Way’s tidal field weakens with galactocentric distance, it is expected that mass loss due to tidal effects follows a similar trend. Hence, the amount of mass lost by very distant globular clusters

should be less than those moving in the Milky Way bulge. Furthermore for a given orbit, clusters that are more massive or more compact will have a stronger self-gravity and will be less affected by tidal heating. Such behaviour has been observed within the old globular clusters of the Large Magellanic Cloud, where the galaxy’s gravitational potential seems to act differently as a function of the cluster distance from the galaxy’s centre (Piatti & Mackey 2018).

From a purely theoretical approach, the literature is rich with studies on how star clusters are affected by the tidal field of their host galaxy (e.g. Gnedin et al. 1999; Lamers et al. 2005; Heggie & Hut 2003; Renaud et al. 2011; Baumgardt & Makino 2003; Gieles & Baumgardt 2008; Kruijssen & Mieske 2009; Webb et al. 2013, 2014). Most applicable to this study is the work done by Baumgardt & Makino (2003), who performed N-body simulations to study how a spherically symmetric external tidal field, in addition to stellar evolution and two-body relaxation, affects the evolution of a star cluster’s mass function. They found that mass segregation leads to low-mass stars being preferentially stripped from star clusters, which causes mass functions that initial

* E-mail: andres.piatti@unc.edu.ar

increase towards the low-mass end to begin decreasing towards the low-mass end (see [Webb et al. 2017](#), for a direct comparison to observations). From their suite of simulations, [Baumgardt & Makino \(2003\)](#) were also able to generate a relation for estimating a cluster’s dissolution time based on its orbit in the galaxy. Expectedly, inner region clusters are expected to dissolve faster than outer region clusters. A secondary dependence exists in the form of the cluster’s orbital eccentricity, with clusters that have high orbital eccentricities reaching dissolution faster than clusters with low orbital eccentricities but comparable apocenters. It should be noted that the simulations were limited to approximately 10^5 particles. More massive clusters will have less two body relaxation, $\propto \log N/N$. Tidal heating, which depends on the cluster size, has no dependence on particle mass.

For cluster’s in non-spherically symmetric tidal fields, tidal heating can also occur in the form of shocks. [Spitzer \(1958\)](#) was the first to study the disruption of clusters due to tidal shocks, and found the amount of mass lost mainly depends on the strength of the shock and the cluster’s density within its half-mass radius. Giant molecular clouds (GMCs) are now known to be the dominant source of mass loss over a cluster’s lifetime ([Gieles et al. 2006](#); [Lamers & Gieles 2006](#); [Kruijssen et al. 2011](#); [Gieles & Renaud 2016](#)), primarily affecting clusters when they first form and the local GMC encounter rate is high. Focussing on disc shocks in particular, studies have shown that repeated passages through the Galactic disc will accelerate a cluster’s dissolution time relative to a cluster orbiting in the plane of the disc ([Gnedin & Ostriker 1997](#); [Gieles et al. 2007](#); [D’Onghia et al. 2010](#); [Kruijssen et al. 2011](#); [Webb et al. 2014](#)). Other forms of substructure, including galaxy merger-induced structure ([Kruijssen et al. 2012](#)) and dark matter sub-halos ([Webb et al. 2019](#)) can also subject a cluster to a tidal shock.

Finally, an additional factor that makes it difficult to estimate a cluster’s mass-loss history based on its orbit alone is the fact that a significant fraction of the Galactic cluster population has been accreted ([Massari et al. 2019](#)). Hence these clusters have not been on their current orbit for their entire lifetime, and could have lost significantly more (or less) mass than one would predict given their current orbit and structural properties. Luckily the structural properties of accreted clusters are expected to respond to the tidal field of their new host, in this case the Milky Way, very quickly ([Miholics et al. 2014](#)).

Historically, studies of how Galactic globular clusters have been affected by the Milky Way have been limited by the fact that their orbits were unknown. Hence conclusions could only be drawn based on their observed properties and their present galactocentric distance. Furthermore, estimates of a cluster’s mass and size were taken from a wide range of inhomogenous studies. As the proper motions of select globular clusters started becoming available, a proper analysis of how individual Galactic globular clusters have been affected by tides was possible ([Dinescu et al. 1999](#); [Kruijssen & Mieske 2009](#); [Webb et al. 2012](#); [Balbinot & Gieles 2018](#)). In some cases, it was even possible to determine if a cluster’s evolution was dominated by two-body relaxation or tidal stripping ([Dinescu et al. 1999](#)). Unfortunately, similar to catalogues of globular cluster structural parameters, estimates of cluster orbits were inhomogeneous and typically incomplete. Hence it has been difficult for past

studies to identify how strongly a cluster’s evolution has been affected by the tidal field of its host galaxy.

With the most recent data release from the European Space Agency’s *Gaia* satellite (DR2), the orbit of every Galactic globular cluster is now known ([Gaia Collaboration et al. 2018](#); [Vasiliev 2019](#); [Baumgardt et al. 2019](#)). Combining data from *Gaia* DR2 with ground-based line-of-sight velocities and estimates of each cluster’s mass and size ([Baumgardt & Hilker 2018](#)), [Baumgardt et al. \(2019\)](#) was able to derive the mass lost by each globular cluster since formation by integrating their orbits backwards in time and accounting for dynamical friction.

The [Baumgardt et al. \(2019\)](#) catalogue, which contains cluster positions, space velocities, orbital motion parameters, structural properties, and initial masses of almost all known Milky Way globular clusters ([Harris 1996](#), 2010 December edition) is the most suitable database for studying the extent that the observed structural properties of clusters have been affected by the Milky Way’s tidal field. Hence the purpose of this study is to make use of the [Baumgardt et al. \(2019\)](#) catalogue to analyse how the Milky Way’s gravitational field affects various observable properties of globular clusters. The estimated fraction of cluster mass lost by disruption serves as a tracer of how strongly a cluster is tidally affected, which can then be compared to several structural and dynamical parameters in order to help constrain a cluster’s origin (*in-situ* vs accreted), its properties at formation, and whether or not its evolution is dominated by internal or external processes.

The catalogue allows for a homogeneous comparison of a cluster’s structural and orbital properties, while also providing an estimate of what each cluster’s mass was at formation. This type of study is only possible because Galactic globular clusters are born at the earliest epochs of the Milky Way formation ([Kruijssen 2014](#); [Kruijssen et al. 2018](#)) and, consequently, their mass lost due to evolutionary effects is in practice the same (e.g. [Lamers et al. 2005](#)). Therefore, it can be expected that any difference between their structural parameters could be due to the difference tidal forces acting on them.

In Section 2 we introduces the data set used in this work. In Section 3, we explore how the estimated fraction of mass lost by each cluster is related to its orbit, several tracers of cluster size, its density profile, dynamical age, and tidal filling factor. Finally, in Section 4 we summarise the main conclusions of this work.

2 DATA HANDLING

To explore how strongly tides have shaped a cluster’s evolution, we make use of the Galactic positions (X, Y, Z), space velocities (U, V, W), perigalactic (R_{peri}) and apogalactic (R_{apo}) distances, and initial (M_{ini}) and current (M_{GC}) masses of 156 Milky Way globular clusters as derived by [Baumgardt et al. \(2019\)](#). In their study, [Baumgardt et al. \(2019\)](#) estimates cluster positions and velocities using data from *Gaia* DR2. R_{peri} and R_{apo} are then determined by integrating the cluster’s orbits assuming the [Irrgang et al. \(2013\)](#) model of the Milky Way. The structural properties of each cluster, mainly their core (r_c) and half-mass (r_h) radius, are taken from [Baumgardt & Hilker \(2018\)](#) who estimate the

values by comparing the density profiles of Galactic globular clusters to a large suite of direct N -body star cluster simulations. Since the set of orbital and structural cluster properties have been derived by applying the same methodology, the catalogue represents the largest homogeneous, up-to-date data set of the Milky Way globular cluster system. It is useful to note that Baumgardt et al. (2019) uses Irrgang et al. (2013)'s model for the Milky Way in order to solve for each cluster's R_{peri} and R_{apo} . This model consists of a Plummer sphere bulge, a Miyamoto & Nagai (1975) disc, and a modified Allen & Santillan (1991) dark matter halo. We also performed an independent orbit integration for each cluster using the commonly cited MWPotential2014 Galactic model (Bovy 2015), which consists of a bulge that is represented by a spherical power-law potential, a Miyamoto & Nagai (1975) disc, and a Navarro et al. (1997) halo. A comparison revealed only minor differences between the orbital parameters of clusters orbiting in the innermost regions of the Milky Way (which is poorly constrained).

It is important to note that the M_{ini} values in Baumgardt et al. (2019) were obtained by integrating each cluster's orbit backwards in time from their observed positions and space velocities and measured current masses, taking into consideration the dynamical drag force. Using the formalism of Baumgardt & Makino (2003), the authors were able to estimate the mass loss via tidal stripping. It was additionally assumed that clusters lose half of their M_{ini} due to stellar evolution during their first gigayear (see also de Grijs et al. 2005). Baumgardt et al. (2019) iterated over a wide range of M_{ini} values until they were able to recover each cluster's M_{GC} , on the basis of a linear mass loss dependence with time in a spherically symmetric, isothermal galaxy potential over the entire age of each cluster (see also Lamers et al. 2010). One should allow for a dispersion in the fraction of mass lost by disruption of ~ 15 -20 per cent due to the uncertainty in the cluster's ages (Helmi et al. 2018; Pfeffer et al. 2018). M_{ini} should also be taken to be a lower limit for several reasons. First, it does not take into account early mass lost by the cluster before it leaves its formation environment and reaches its present day orbit (Kruijssen 2015). Second, interactions with GMCs, which have been shown to be the dominant source of cluster mass loss at early times (Gieles et al. 2006; Kruijssen et al. 2011), are also not included in the calculation. Note that accreted clusters were likely not harassed as much by GMCs as *in-situ* clusters, while clusters formed in the inner part of the Milky Way likely encountered more GMCs than those formed in the outskirts. Notice also that the strength of the tidal field is expected to increase, on average, with cosmic time as the Milky Way grows (Renaud et al. 2017), and that the presence of the bar (Rossi et al. 2018) and spiral arms (Gieles et al. 2007) will accelerate mass loss as well, which is not considered in Baumgardt et al. (2019). Therefore, the estimates of initial mass used in this work are lower limits as many mass-loss mechanisms are not included. In fact, initial mass estimates are perhaps more accurately tracers of the tidal field strength associated with a cluster's current orbit in the present day potential of the Milky Way.

From the above data set, we computed the semi-major axis of each globular cluster's orbit:

$$a = \frac{R_{peri} + R_{apo}}{2}. \quad (1)$$

The semi-major axis has the advantage of having no time-dependence, as opposed to the cluster's current Galactocentric distance, and is more representative of the mean orbital distance of the globular clusters than R_{peri} or R_{apo} . We also computed the orbital eccentricity (ϵ) as:

$$\epsilon = \frac{R_{apo} - R_{peri}}{R_{apo} + R_{peri}}, \quad (2)$$

and the values of Jacobi radii from the expression (Chernoff & Weinberg 1990):

$$r_J = \left(\frac{M_{GC}}{3M_{MW}} \right)^{1/3} \times a, \quad (3)$$

where M_{MW} is the Milky Way mass contained within the semi-major axis of the cluster's orbit, which is different for each cluster. In order to estimate M_{MW} we used the same Irrgang et al. (2013) Milky Way mass profile that Baumgardt et al. (2019) used to solve the orbit of each cluster. We note that a and e are calculated in a galaxy model that is fitted to the present day properties of the Milky Way. However, the Milky Way has been grown over time, so that a and e have not been the same over the course of a cluster's lifetime.

Finally, to estimate how much clusters have been disrupted due to relaxation and tidal heating, we split the difference between M_{ini} and M_{GC} up between mass lost via stellar evolution (M_{ev}) and mass lost due to disruption (M_{dis}):

$$M_{ini} = M_{GC} + M_{ev} + M_{dis}, \quad (4)$$

with $M_{ev} = 0.5 \times M_{ini}$, from which we get:

$$M_{dis}/M_{ini} = 1/2 - M_{GC}/M_{ini}. \quad (5)$$

Hence eq.(5) explicitly gives the fraction of cluster mass lost by relaxation and tidal heating as computed (but not tabulated) by Baumgardt et al. (2019). In their study, the authors' only considered the relationship between M_{GC} , M_{ini} and Galactocentric distance (see their Figure 7). In the subsequent analysis we use M_{dis}/M_{ini} as the indicator for tidal field strength.

We estimated the uncertainties of each derived parameter $f(x_1, x_2, \dots, x_n)$ on the basis of Monte Carlo simulations. We run one thousand calculations of $f(x_1, x_2, \dots, x_n)$ for each globular cluster with random distributions of each independent variable x_i over the interval $x_i \pm \sigma(x_i)$, for $i = 1, \dots, n$, where $\sigma(x_i)$ is the error associated to x_i according to Baumgardt et al. (2019). From the resulting distribution of the one thousand generated values, we set the uncertainty of each parameter equal to the range encompassing the central 16% and 84% points.

3 ANALYSIS AND DISCUSSION

We begin our analysis of the Baumgardt & Hilker (2018) and Baumgardt et al. (2019) data with Fig. 1, which depicts the relationship between orbital eccentricity, the cluster’s semi-major axis and the fraction of mass lost by disruption. Fig. 1 shows that M_{dis}/M_{ini} is a function of both the semi-major axis and the eccentricity. Likewise, for a given semi-major axis, it is also apparent that the larger the eccentricity of a cluster’s orbit the larger the fraction of mass lost by disruption, as eccentric clusters are brought deeper into the Milky Way’s potential well. We note that while this result is simply a byproduct of employing Baumgardt & Makino (2003) to estimate each cluster’s initial mass, but it is worth illustrating such a relationship for the actual Milky Way globular cluster system. Highly eccentric clusters are also likely have higher orbital inclinations – consistent with Piatti (2019) –, meaning they should dissolve even quicker than estimates by Baumgardt et al. (2019) due to disc shocking (Webb et al. 2014). In fact, Piatti (2019) found that ~ 30 per cent of globular clusters are on orbits with an inclination angle between 20° and 50° . The majority of clusters have even higher inclinations that exceed 50° . Hence most Galactic globular clusters have undergone several disc crossing compared to those orbiting on more circular orbits in the plane of the disc at a similar distance from the Milky Way centre. Clusters with highly inclined orbits will of course lose more mass (Gnedin et al. 1999; Webb et al. 2014).

Just as interesting are the regions of Fig. 1 where no globular clusters are observed. In general Milky Way bulge globular clusters ($\log(a/\text{kpc}) < 0.5$) with orbits’ eccentricities smaller than ~ 0.5 make up a minor percentage of the total population, as is also the case for outermost ones ($\log(a/\text{kpc}) > 1.5$ with eccentricities smaller than ~ 0.5). This behaviour would seem to be an intrinsic property of the Milky Way globular cluster system, however likely for different reasons. Bulge clusters are subjected to a very strong tidal field, and therefore expected to lose mass quickly and will likely dissolve within a Hubble time if they are not extremely massive and compact. Hence the few existing inner region clusters with eccentricities smaller than ~ 0.5 represent the tail end of the initial globular cluster mass and size distributions.

The lack of outer clusters with low eccentricities is consistent with recent work by Piatti (2019), who studied the kinematics properties of the Milky Way globular cluster system and found that outer globular clusters, independent of the direction of their motions (prograde or retrograde orbits), tend to have more radial orbits than those in the disc of the Milky Way and preferentially have large orbital inclination angles. Piatti (2019) also showed that only outer globular clusters that form *in-situ* with their host will have radial orbits, accreted globular clusters will have radial orbits regardless of their location in the Milky Way. Finally, by assigning the same probability to an accreted globular cluster to have a prograde or a retrograde orbit, Piatti (2019) found that the accreted to *in-situ* globular cluster ratio turns out to be ~ 1 . Hence the lack of outer clusters with low eccentricities is likely due to the fact that most outer halo clusters have been accreted via a past merger. So while the lack of inner region clusters with low eccentricities is due to cluster disruption, the lack of outer region clusters with low

eccentricities is likely due to no clusters ever forming there in the first place.

Finally, we also see a region in the top left region of Fig. 1 where no clusters currently exist that extends out to $(\log(a/\text{kpc}) \sim 1.0$. The lack of clusters in this portion of the diagram can again be attributed to cluster disruption, as a small semi-major axis and high orbital eccentricity would bring a cluster deep into the Galaxy’s potential well. Hence any cluster that formed with this orbit would dissolve quickly. A puzzling population exists however with intermediate eccentricities ($0.5 < e < 0.8$) and small semi-major axes ($\log(a/\text{kpc}) < 0.5$), which Baumgardt et al. (2019) predicts must have been very massive at birth in order to survive a Hubble time. While it is entirely possible these are simply some of the most massive clusters every to have formed in the Milky Way, an alternative explanation would be that these clusters did not always have their present day orbit. Inward migration is typically due to either dynamical friction or an accretion event. In the dynamical friction scenario, which Baumgardt et al. (2019) accounts for, the clusters were born very massive and have had their orbits decay from a weaker tidal field to a stronger one. Hence they have not spent their entire lifetime subjected to weak tides. In the accretion scenario, a cluster initially orbit deep in the potential well of a dwarf and is not stripped until its previous host reaches the inner parts of the Milky Way and is near dissolution. In this latter scenario the cluster still orbits in a strong tidal field for the majority of its life, but while a member of a dwarf galaxy the tidal field may be compressive (Bianchini et al. 2015; Webb et al. 2017b).

In order for these GCs to migrate inwards, from a weaker tidal field to the strong one they experience at present day, they were likely subject to 1 of 2 mechanisms. Either they were very massive at birth and strongly affected by dynamical friction (which Baumgardt accounts for). Or they were accreted clusters that orbited in the inner regions of a dwarf galaxy. Hence it was not until their previous host reached the inner Milky Way and was almost completely disrupted that they were accreted.

The different tidal field strengths experienced by globular clusters will also affect their structural parameters, and ultimately their internal dynamical evolutionary stages, with respect to what is expected while evolving in isolation. Figs. 2-4 illustrate the relationships between r_c , r_h and r_J with the semi-major axis and the fraction of mass lost by disruption, respectively. The three figures highlight a general trend, in the sense that any of the derived radii increase as a function of the cluster distance from the Milky Way centre. This outcome was predicted theoretically by Hurley & Mackey (2010) and Bianchini et al. (2015), among others. Globular clusters in weaker tidal fields, like those located in the outermost regions of the Milky Way can expand naturally, whereas those immersed in stronger tidal fields (e.g., the Milky Way bulge) do not. Hence we see a wider spread in cluster sizes at larger galactocentric distances than in the inner regions of the Galaxy. We also see an absence of significant outliers in these figures due to accreted clusters, as Miholics et al. (2014) has shown the size of an accreted cluster will quickly respond to the tidal field of the Milky Way.

When comparing Figs. 2-4, some more subtle differences do arise. More specifically, r_c , r_h and r_J all increase with semi-major axis at different paces and the spread in radius

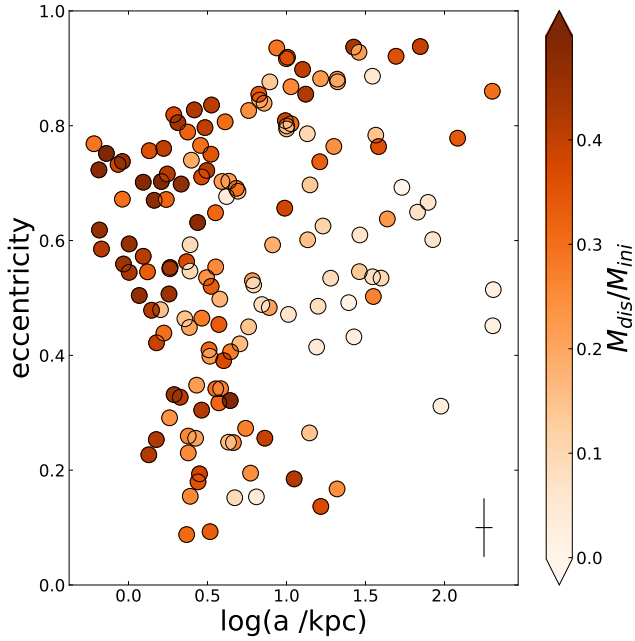


Figure 1. Relationship between the eccentricity, the semi-major axis and the fraction of disrupted mass for the Baumgardt et al. (2019)’s globular cluster sample. Typical error bars are indicated.

at a given $\log(a / \text{kpc})$ is also different. Indeed, r_c is the radius which increases the slowest with $\log(a / \text{kpc})$, while r_J shows the fastest growth. This behaviour is particularly noticeable for globular clusters inside a circle of 10 kpc ($\log(a / \text{kpc}) < 1.0$). For instance, the mean r_c , r_h and r_J values at $\log(a / \text{kpc}) = 1$ are 2, 5 and 10 times those at $\log(a / \text{kpc}) = -0.3$, respectively. This result expectedly indicates that the innermost regions of globular clusters are less sensitive to external changes in the Milky Way gravitational field. Similarly, with the cluster’s inner regions being less affected by tides than its outer regions, we observe a larger spread in r_c than we do for r_h and r_J . Since outer region clusters are less affected by the tidal field, with most likely not having expanded to the point of becoming tidally filling (Hénon 1961; Alexander & Gieles 2013), the rate of increase in r_c , r_h and r_J is primarily the result of the initial size and mass distribution of globular clusters and the combined effects of stellar evolution and two-body relaxation. Similar trends are detected in the ancient globular clusters of the Large Magellanic Cloud (Piatti & Mackey 2018), whose sizes, Elson et al. (1987)’s power-law slopes at large radii (γ , Mackey & Gilmore 2004), ratios of the cluster radius to Jacobi radius, and the inverse of the concentration parameter c increase with the deprojected galactocentric distance. Similar trends are also seen in giant elliptical galaxies (Harris 2009; Webb et al. 2016).

Heggie & Hut (2003) have described the internal dynamics evolution of a star cluster as seen in the r_c/r_h versus r_h/r_J plane. As a star cluster expands to the point of being tidally filling, it experiences violent relaxation in its core region followed by two-body relaxation, mass segregation and finally core-collapse. These processes result in clusters evolving from having high r_c/r_h and low r_h/r_J to low r_c/r_h and high r_h/r_J . We examined such a diagnostic diagram for our

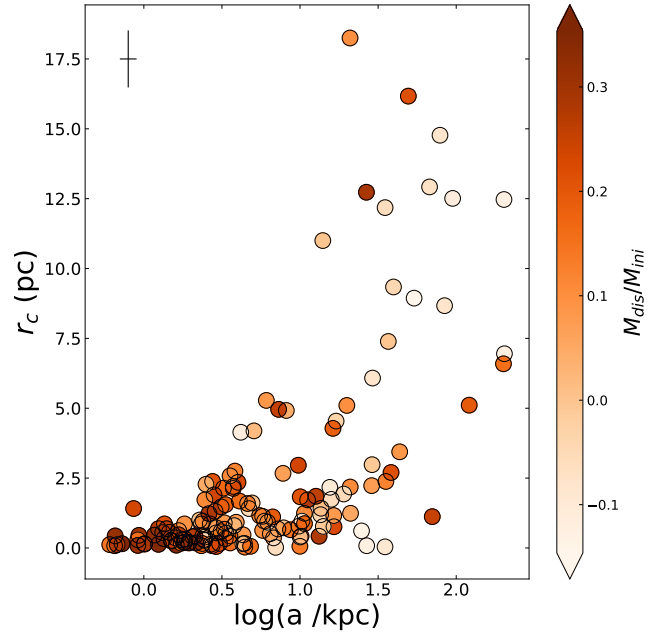


Figure 2. Relationship between the core radius, the semi-major axis and the fraction of mass lost by disruption for the Baumgardt et al. (2019)’s globular cluster sample. Typical error bars are indicated.

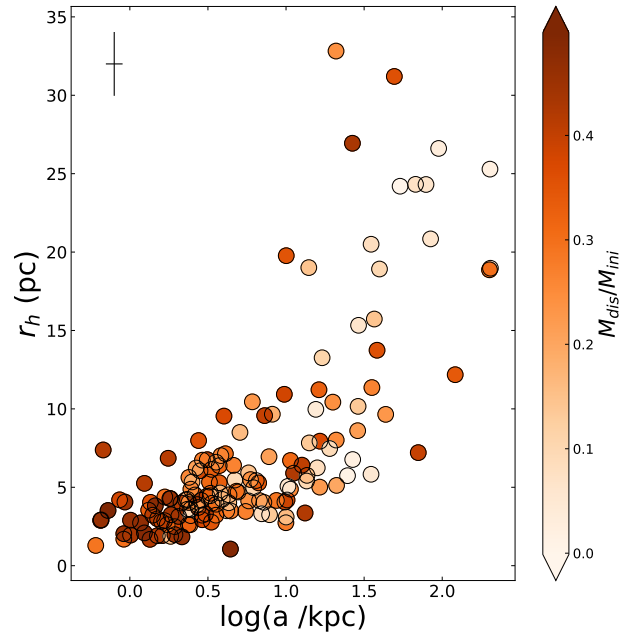


Figure 3. Relationship between the half-mass radius, the semi-major axis and the fraction of mass lost by disruption for the Baumgardt et al. (2019)’s globular cluster sample. Typical error bar is indicated.

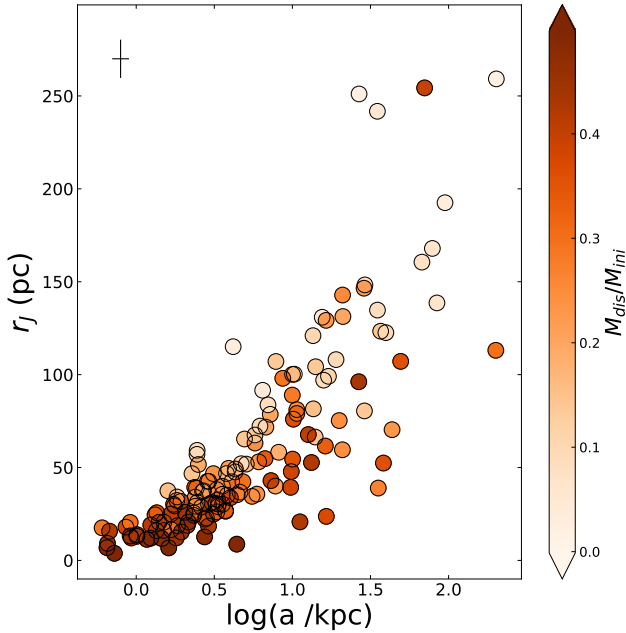


Figure 4. Relationship between the Jacobi radius, the semi-major axis and the fraction of mass lost by disruption for the Baumgardt et al. (2019)’s globular cluster sample. Typical error bars are indicated.

156 globular cluster sample and connect the observed trends with those of Figs. 1-4 by using the same colour scale given by the range of M_{dis}/M_{ini} . We find that the Milky Way’s tidal field has had a role in shaping the internal dynamical evolution of clusters as well.

Fig. 5 shows that core-collapse globular clusters are mainly Milky Way bulge objects ($\log(a / \text{kpc}) \lesssim 0.5$). They occupy the region delimited by $r_c/r_h \lesssim 0.2$ and $r_h/r_J \gtrsim 0.30$. Likewise, the least dynamically evolved globular clusters would appear to be the outermost ones ($r_c/r_h \gtrsim 0.45$). Although globular clusters have been born with different masses and sizes, and hence they should stay at different internal dynamics stages even if they were evolved in isolation, the fact that those at a more advanced dynamical stage are the ones located in inner Milky Way regions reveals that the Milky Way potential well has differentially accelerated their internal dynamical evolution. Having lost a large fraction of their initial masses and having their sizes tidally limited will minimize an inner region cluster’s relaxation time, allowing it to evolve quickly compared to outer region clusters which lose little mass and can expand to large sizes. Note, for instance, that globular clusters that have lost more than 45 per cent of their masses by disruption are mostly bulge globular clusters at an advanced evolutionary stage, and conversely, those with $M_{dis}/M_{ini} \lesssim 0.10$ – located in the outermost Milky Way regions – are relatively less evolved globular clusters. Some degeneracy exists, of course, as some clusters were likely to have been more with short initial relaxation times and reached the core-collapse phase simply through rapid relaxation. The mostly likely candidates for having their evolution be internally (relaxation) driven as opposed to through interactions with the tidal field are cluster with

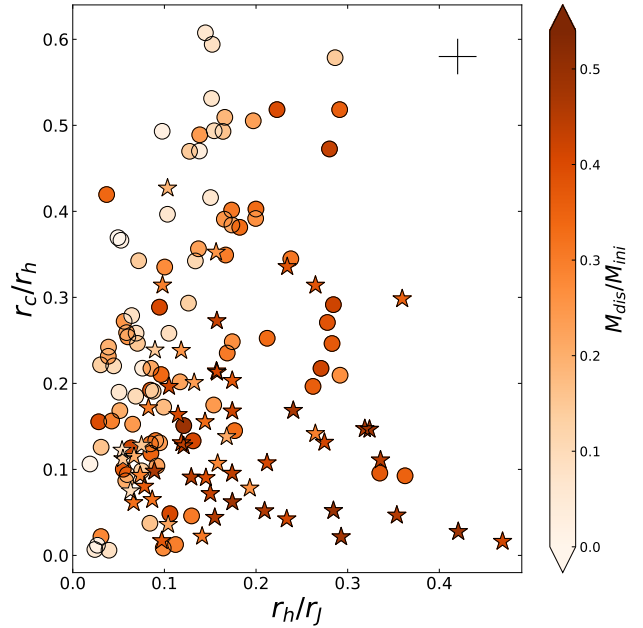


Figure 5. Relationship between r_c , r_h and r_J radii. Typical error bars are indicated. Filled stars and circles represent clusters located inside and outside the bulge volume ($\log(a / \text{kpc}) = 3$), respectively.

low r_c/r_h that are not predicted to have lost much mass via tidal stripping (lighter points).

Further evidence of such a differential acceleration of the globular cluster internal dynamics evolution is depicted in Fig. 6, where we plot the fraction of mass lost by disruption as a function of the ratio between each cluster’s age and its half-mass relaxation time (age/t_{rh}). Value for t_{rh} are taken from Baumgardt et al. (2019), where t_{rh} is calculated using the formalism of Baumgardt & Hilker (2018). Globular cluster ages were assumed to be $12_{-2.0}^{1.5}$ Gyr (Kruijssen et al. 2018). As can be seen in Fig. 6, globular clusters with $M_{dis}/M_{ini} \gtrsim 0.45$ ($\log(a / \text{kpc}) \lesssim 0.5$) have apparently lived many more median relaxation times than their more remote counterparts ($M_{dis}/M_{ini} \lesssim 0.10$, which corresponds to $\log(a / \text{kpc}) \gtrsim 1.5$). The small or negligible amount of mass lost by disruption of the outermost globular clusters lead us to conclude that most of the amount of mass lost during their lifetimes should have been by relaxation. Even for a given dynamical age, there is a clear spread in M_{dis}/M_{ini} that can be attributed to cluster orbit (as traced by each cluster’s semi-major axis in the color-bar). This spread helps separate between whether or not a cluster’s dynamical age is the result of its formation properties or tidal interactions.

Fig. 6 also shows that globular clusters that have lost between 15 and 40 per cent of their masses by disruption have similar dynamical ages. These globular clusters mostly populate the Milky Way disc ($0.5 \lesssim \log(a / \text{kpc}) \lesssim 1.4$), so that the range of mass fraction lost is primarily linked to the globular cluster’s distance from the Galactic centre. We checked whether globular clusters with highly eccentric orbits could have affected their age/t_{rh} ratios because of their many disc crossings, and found that they do not differentiate from those with smaller eccentricities. Indeed, Fig. 1 shows

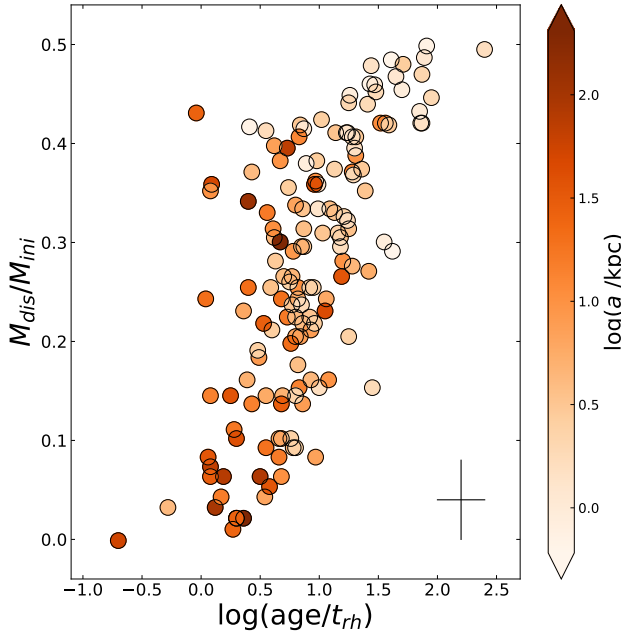


Figure 6. Globular cluster fraction of mass disrupted by tidal effects as a function of the age/ t_{rh} ratio. Typical error bars are indicated.

that globular clusters with eccentricities > 0.8 have lost between ~ 15 and 45 per cent of their masses by disruption, a M_{dis}/M_{ini} range where $\log(\text{age}/t_{rh})$ is nearly constant (0.75 ± 0.25 , see Fig. 6).

Baumgardt et al. (2010) investigated the r_h/r_J ratio of Galactic globular clusters as given by the Milky Way’s potential and found that the r_h/r_J ratio is a good discriminator between globular clusters that are compact and extended at birth. This ratio has also long been the criteria for determining whether a cluster is tidally filling or not, with clusters that have $r_h/r_J > 0.145$ considered to be tidally filling (Hénon 1965). Baumgardt et al. (2010) found that for Galactocentric distances larger than 8 kpc, r_h/r_J ratios smaller than 0.05 correspond to initially compact objects, while r_h/r_J ratios between 0.1 and 0.3 point to globular clusters intrinsically larger, and not because of expansion in a weaker tidal field. Both groups of globular clusters would have an *in-situ* origin. To further expand their study on compact and extended clusters, in the left panel of Fig. 7 we reproduce Baumgardt et al. (2010)’s figure 2 comparing r_h/r_J to each cluster’s semi-major axis for our enlarged globular cluster sample. In order to make Fig. 7 as informative as possible, we included some other cluster orbital motion parameters, namely, the orbit eccentricity and inclination; the latter split in arbitrary bins. In both panels, symbol sizes are proportional to each cluster’s orbital eccentricity and symbol shapes are related to their orbital inclinations (i). For comparison purposes we also show in the right panel r_h/r_J versus each cluster’s perigalactic distance, where in this case r_J is calculated at perigalactic.

For reference purposes, we include Table 1 in the Appendix containing all the relevant information used in making Figure 7. Table 1 serves as a useful source for identifying clusters that are tidally filling or under-filling both on

average and near pericentre. Clusters that are tidally under-filling at pericentre have likely had their evolution governed by two-body relaxation, while clusters that are on average tidally filling have likely had their evolution strongly shaped by the tidal field. For all other clusters, a combination of relaxation and tidal interactions have played a role in their evolution and it’s not necessarily the case that one mechanism is more dominant over the other.

The left panel of Fig. 7 shows that, in general, the smaller the distance from the Milky Way centre the larger the r_h/r_J ratio. This would seem to be a consequence of inner region clusters easily expanding to the point of being tidally filling due to stellar evolution and two-body relaxation. Hence they have experienced a significant amount of mass loss due to disruption, primarily of low-mass stars that have segregated outwards, leaving the surviving globular clusters with their more massive members (Baumgardt & Makino 2003; Khalisi et al. 2007). Therefore as expected, their M_{dis}/M_{ini} ratios are amongst the largest in the dataset. In the inner regions of the galaxy there is significant scatter about this general trend, as first pointed out by Baumgardt et al. (2010), which is likely a remnant of the range of initial masses and sizes clusters can have at birth.

In the outer regions of the galaxy (beyond ~ 8 kpc), tidally under-filling clusters continue to follow the general trend of r_h/r_J with galactocentric distance down to a mean value of 0.05. Given the relatively weak external tidal field that these clusters are subject to, their evolution is almost entirely dominated by internal processes. However, beyond 8 kpc there also exists a population of tidally filling clusters. Previous work by Baumgardt et al. (2010) also recognized that outer region clusters with $\log(a / \text{kpc}) > 0.9$ could be separated into tidally under-filling ($r_h/r_J < 0.05$) and filling ($0.1 < r_h/r_J < 0.3$) populations. We further separate the filling clusters into two additional sub-populations, with $r_h/r_J \sim 0.2$ (barely tidally filling) and $r_h/r_J \geq 0.3$ (tidally over-filling), based on an apparent gap in the r_h/r_J distribution of outer region clusters. Given the relatively weak tidal field the clusters experience, tidally filling outer region clusters are likely to either be accreted, have high eccentricities, or formed quite extended.

Independent of semi-major axis, we identify a potential third group of globular clusters with $0.4 < r_h/r_J < 1.0$. Clusters in this group also have highly eccentric and inclined orbits, such that they are subject to strong tidal shocks at pericentre and during disc passages. Given that these four clusters are severely tidally over-filling, they should be in the process of dissolving.

The right panel of Fig. 7 is also of interest, as it indicates that almost every cluster is tidally filling at perigalacticon. Hence, while the few that are not tidally filling at perigalacticon can be considered to have had their evolution be relaxation dominated, the majority of clusters are affected by the tidal field to some degree. Clusters that are tidally filling at their semi-major axis (left panel) are most likely to have their evolution be tidally dominated.

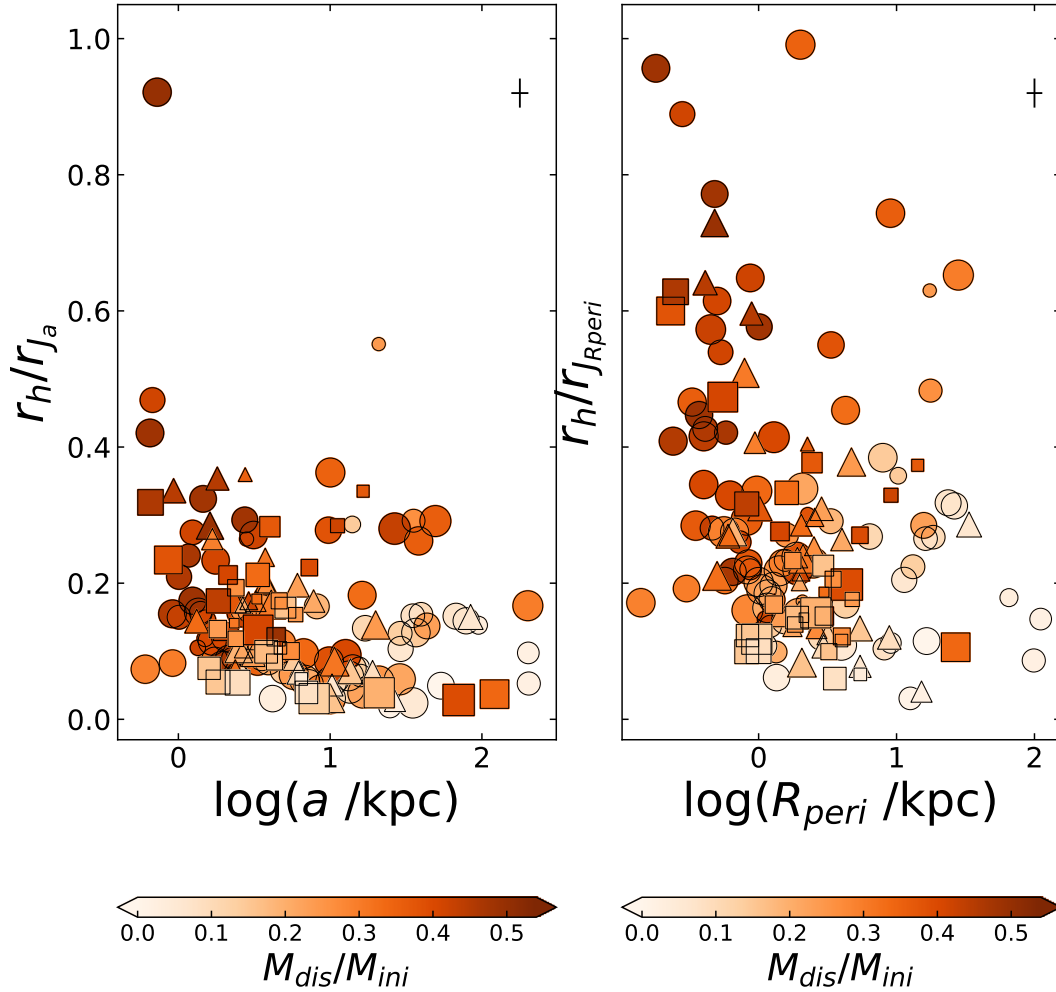


Figure 7. Left Panel: r_h/r_J compared to each cluster’s semi-major axis, where r_J is calculated at the cluster’s semi-major distance. Right Panel: r_h/r_J compared to each cluster’s pericentre, where r_J is calculated at the cluster’s perigalactic distance. Typical error bars are indicated. According to [Baumgardt et al. \(2010\)](#), globular clusters located at Galactocentric distances > 8 kpc and below $r_h/r_J = 0.1$ or $0.1 < r_h/r_J < 0.3$ are genuine compact and extended objects at birth, respectively. Symbol sizes are proportional to the orbit eccentricities ($0 < \epsilon < 1$), while triangles, squares and circles correspond to orbit inclinations (i) between $i \leq 30^\circ$, $30^\circ < i \leq 60^\circ$ and $i > 60^\circ$, respectively.

4 CONCLUSIONS

We have analysed the relationships between the Milky Way’s globular clusters structural parameters, their internal dynamical stages, and the the fraction of mass lost by tidal effects (disruption). There has long been a general understanding that the Milky Way gravitational field has played a strong role in the globular cluster mass loss process along their lifetimes.

We made use of publicly available positions, space velocity components, orbital motion parameters, core, half-mass and tidal radii, relaxation times, current and initial masses of 156 Milky Way globular clusters, from which we addressed the issue about at what extend the Milky Way potential well has acted in shaping their present-day sizes and dynamical age. As suggested by previous theoretical results, we started by analysing the relationship between the fraction of mass

lost by disruption, the globular cluster distance to the Milky Way centre and the eccentricity of their orbits. We find an absence of cluster with short semi-major axes and either low or high orbital eccentricities, likely due to the fact that any clusters born in this regime would reach dissolution fairly quickly. Although a puzzling population of clusters with intermediate eccentricities and short semi-major axes is observed, also with relatively high orbital inclinations. There is also a lack of outer region clusters with low orbital eccentricities, likely due to outer region clusters primarily being accreted clusters that have orbits that are comparable to the radial orbit in which their progenitor host galaxy fell in on.

The core, half-mass and Jacobi radii of Galactic clusters show different rates of increase with Galactocentric distance, in the sense that the core radii increases slower than the half-mass radii, which in turn increases at a slower pace than Jacobi radii. This outcome would seem to suggest that the

inner most regions of globular clusters are less sensitive to changes in the Milky Way potential with the Galactocentric distance. On the contrary, their outermost regions would appear more vulnerable.

From the different fractions of mass lost by disruption of each cluster, we found that the Milky Way's gravitational field has differentially accelerated the internal dynamical evolution of its globular clusters. Having been stripped of a large fraction of their initial mass, and having their sizes tidally limited, inner region clusters will have shorter relaxation times than outer region clusters. Hence globular clusters located in the bulge would seem to be at a more advanced internal dynamical evolutionary stage, approaching to or at the core-collapse stage, while more distant globular clusters have lived many fewer median relaxation times than their innermost counterparts.

Finally, we confirmed the existence of two intrinsically different size globular cluster groups as identified by Baumgardt et al. (2010) at large Galactocentric distances. That is to say we find globular clusters can primarily be split into groups with $r_h/r_J \sim 0.05$ and 0.20 that have lost a very small fraction of their initial mass. However, we point out that interspersed within both groups are clusters that have lost a large percentage of their masses by disruption. Hence it is more difficult to distinguish between clusters that are compact and extended at birth from their r_h/r_J ratio alone. There is a third group of objects with $r_h/r_J > 0.4$ which have lost even more mass due to tidal effects. In both cases, clusters that have lost a large portion of their initial mass have highly eccentric orbits with large inclination angles, which leads to them experiencing more tidal shocks at perigalcticon and while crossing the disc. Hence they have lost an additional fraction of mass over what their semi-major axis alone implies. These clusters are, most likely, clusters that have been accreted by the Milky Way and have had their structural properties respond to their new host.

ACKNOWLEDGEMENTS

We thank the referee, Florent Renaud, for a timely and constructive report to improve the manuscript. We thank Henny J.G.L.M. Lamers and Mark Gieles for their reading through an earlier version of this manuscript and timely comments and Holger Baumgardt for providing us with his globular cluster database.

REFERENCES

- Alessandrini E., Lanzoni B., Miocchi P., Ciotti L., Ferraro F. R., 2014, *ApJ*, **795**, 169
- Alexander P. E. R., Gieles M., 2013, *MNRAS*, **432**, L1
- Allen C., Santillan A., 1991, *Revista Mexicana de Astronomia y Astrofisica*, **22**, 255
- Balbinot E., Gieles M., 2018, *MNRAS*, **474**, 2479
- Baumgardt H., Hilker M., 2018, *MNRAS*, **478**, 1520
- Baumgardt H., Makino J., 2003, *MNRAS*, **340**, 227
- Baumgardt H., Parmentier G., Gieles M., Vesperini E., 2010, *MNRAS*, **401**, 1832
- Baumgardt H., Hilker M., Sollima A., Bellini A., 2019, *MNRAS*, **482**, 5138
- Bianchini P., Renaud F., Gieles M., Varri A. L., 2015, *MNRAS*, **447**, L40
- Bovy J., 2015, *ApJS*, **216**, 29
- Brockamp M., Küpper A. H. W., Thies I., Baumgardt H., Kroupa P., 2014, *MNRAS*, **441**, 150
- Chernoff D. F., Weinberg M. D., 1990, *ApJ*, **351**, 121
- D'Onghia E., Springel V., Hernquist L., Keres D., 2010, *ApJ*, **709**, 1138
- Dinescu D. I., Girard T. M., van Altena W. F., 1999, *AJ*, **117**, 1792
- Elson R. A. W., Fall S. M., Freeman K. C., 1987, *ApJ*, **323**, 54
- Fall S. M., Zhang Q., 2001, *ApJ*, **561**, 751
- Gaia Collaboration et al., 2018, *A&A*, **616**, A12
- Gieles M., Baumgardt H., 2008, *MNRAS*, **389**, L28
- Gieles M., Renaud F., 2016, *MNRAS*, **463**, L103
- Gieles M., Portegies Zwart S. F., Baumgardt H., Athanassoula E., Lamers H. J. G. L. M., Sipior M., Leenaarts J., 2006, *MNRAS*, **371**, 793
- Gieles M., Lamers H. J. G. L. M., Portegies Zwart S. F., 2007, *ApJ*, **668**, 268
- Gieles M., Athanassoula E., Portegies Zwart S. F., 2007b, *MNRAS*, **376**, 809
- Gieles M., Heggie D. C., Zhao H., 2011, *MNRAS*, **413**, 2509
- Gnedin O. Y., Ostriker J. P., 1997, *ApJ*, **474**, 223
- Gnedin O. Y., Lee H. M., Ostriker J. P., 1999, *ApJ*, **522**, 935
- Harris W. E., 1996, *AJ*, **112**, 1487
- Harris W. E., 2009, *ApJ*, **699**, 254
- Heggie D., Hut P., 2003, *The Gravitational Million-Body Problem: A Multidisciplinary Approach to Star Cluster Dynamics*
- Helmi A., Babusiaux C., Koppelman H. H., Massari D., Veljanoski J., Brown A. G. A., 2018, *Nature*, **563**, 85
- Hénon M., 1961, *Annales d'Astrophysique*, **24**, 369
- Hénon M., 1965, *Annales d'Astrophysique*, **28**, 62
- Hurley J. R., Mackey A. D., 2010, *MNRAS*, **408**, 2353
- Irrgang A., Wilcox B., Tucker E., Schiefelbein L., 2013, *A&A*, **549**, A137
- Khalisi E., Amaro-Seoane P., Spurzem R., 2007, *MNRAS*, **374**, 703
- Kruijssen J. M. D., 2014, *Classical and Quantum Gravity*, **31**, 244006
- Kruijssen J. M. D., 2015, *MNRAS*, **454**, 1658
- Kruijssen J. M. D., Mieske S., 2009, *A&A*, **500**, 785
- Kruijssen J. M. D., Pelupessy F. I., Lamers H. J. G. L. M., Portegies Zwart S. F., Icke V., 2011, *MNRAS*, **414**, 1339
- Kruijssen J. M. D., Pelupessy F. I., Lamers H. J. G. L. M., Portegies Zwart S. F., Bastian N., Icke V., 2012, *MNRAS*, **421**, 1927
- Kruijssen J. M. D., Pfeffer J. L., Reina-Campos M., Crain R. A., Bastian N., 2018, *MNRAS*,
- Lamers H. J. G. L. M., Gieles M., 2006, *A&A*, **455**, L17
- Lamers H. J. G. L. M., Gieles M., Bastian N., Baumgardt H., Kharchenko N. V., Portegies Zwart S., 2005, *A&A*, **441**, 117
- Lamers H. J. G. L. M., Baumgardt H., Gieles M., 2010, *MNRAS*, **409**, 305
- Mackey A. D., Gilmore G. F., 2004, *MNRAS*, **352**, 153
- Massari D., Koppelman H. H., Helmi A., 2019, arXiv e-prints, p. [arXiv:1906.08271](https://arxiv.org/abs/1906.08271)
- Miholics M., Webb J. J., Sills A., 2014, *MNRAS*, **445**, 2872
- Miyamoto M., Nagai R., 1975, *PASJ*, **27**, 533
- Navarro J. F., Frenk C. S., White S. D. M., 1997, *ApJ*, **490**, 493
- Pfeffer J., Kruijssen J. M. D., Crain R. A., Bastian N., 2018, *MNRAS*, **475**, 4309
- Piatti A. E., 2019, arXiv e-prints, p. [arXiv:1907.09824](https://arxiv.org/abs/1907.09824)
- Piatti A. E., Mackey A. D., 2018, *MNRAS*,
- Renaud F., Gieles M., Boily C. M., 2011, *MNRAS*, **418**, 759
- Renaud F., Agertz O., Gieles M., 2017, *MNRAS*, **465**, 3622
- Rossi L. J., Hurley J. R., Ortolani S., 2018, *MNRAS*, **480**, 1912
- Shukirgaliyev B., Parmentier G., Just A., Berczik P., 2018, *ApJ*, **863**, 171
- Spitzer Lyman J., 1958, *ApJ*, **127**, 17
- Vasiliev E., 2019, *MNRAS*, **484**, 2832

- Webb J. J., Harris W. E., Sills A., 2012, [ApJ](#), **759**, L39
- Webb J. J., Harris W. E., Sills A., Hurley J. R., 2013, [ApJ](#), **764**, 124
- Webb J. J., Sills A., Harris W. E., Hurley J. R., 2014, [MNRAS](#), **445**, 1048
- Webb J. J., Sills A., Harris W. E., Gómez M., Paolillo M., Woodley K. A., Puzia T. H., 2016, [MNRAS](#), **460**, 2129
- Webb J. J., Patel S. S., Vesperini E., 2017b, [MNRAS](#), **468**, 92
- Webb J. J., Vesperini E., Dalessandro E., Beccari G., Ferraro F. R., Lanzoni B., 2017, [MNRAS](#), **471**, 3845
- Webb J. J., Bovy J., Carlberg R. G., Gieles M., 2019, arXiv e-prints, p. [arXiv:1907.13132](#)
- de Grijs R., Parmentier G., Lamers H. J. G. L. M., 2005, [MNRAS](#), **364**, 1054

This paper has been typeset from a $\text{T}_{\text{E}}\text{X}/\text{L}^{\text{A}}\text{T}_{\text{E}}\text{X}$ file prepared by the author.

Table 1. Milky Way globular clusters' parameters used to build Fig. 7.

ID	a (kpc)	R_{peri} (pc)	rh/r_{J_a}	$rh/r_{J_{R_{peri}}}$	ϵ	i (deg)
NGC104	6.45± 0.01	5.46± 0.01	0.06	0.07	0.15±0.00	27.78± 0.80
NGC288	8.17± 0.28	3.33± 0.49	0.17	0.29	0.59±0.05	124.77± 1.83
NGC362	6.76± 0.23	1.05± 0.21	0.06	0.19	0.84±0.03	85.40± 3.63
Whiting1	35.46± 4.48	17.64± 4.08	0.29	0.48	0.50±0.10	71.76± 4.24
NGC1261	10.67± 0.85	1.41± 0.36	0.06	0.22	0.87±0.03	110.52± 9.87
Pal1	16.49± 0.89	14.23± 0.91	0.34	0.37	0.14±0.05	14.45± 5.28
AM1	203.59±89.87	98.84±39.38	0.05	0.09	0.51±0.26	110.20±41.25
Eridanus	84.24±14.67	33.56±23.03	0.15	0.29	0.60±0.22	46.82±28.63
Pal2	20.95± 1.83	2.49± 1.80	0.06	0.23	0.88±0.08	144.05±35.09
NGC1851	9.98± 0.11	0.83± 0.05	0.03	0.16	0.92±0.00	93.82± 1.71
NGC1904	10.15± 0.59	0.82± 0.33	0.06	0.29	0.92±0.03	81.65± 5.22
NGC2298	9.84± 0.73	1.88± 0.79	0.08	0.24	0.81±0.07	121.07± 5.94
NGC2419	53.74± 4.06	16.52± 2.68	0.05	0.11	0.69±0.05	60.48± 6.22
Pyxis	78.74±15.69	26.26± 8.98	0.14	0.31	0.67±0.11	102.92± 3.94
NGC2808	7.85± 0.06	0.97± 0.02	0.03	0.12	0.88±0.00	13.05±20.09
E3	11.18± 1.40	9.11± 0.44	0.28	0.33	0.18±0.10	28.91± 9.65
Pal3	94.87±25.51	65.31±23.15	0.14	0.18	0.31±0.23	71.59±15.90
NGC3201	15.85± 0.61	8.15± 0.09	0.06	0.10	0.49±0.02	152.31± 2.73
Pal4	67.51±14.82	23.66±22.78	0.15	0.32	0.65±0.28	67.95±55.01
Crater	202.23±89.57	110.92±47.45	0.10	0.15	0.45±0.29	109.03±60.62
NGC4147	13.24± 1.32	1.92± 0.77	0.06	0.22	0.86±0.06	83.73± 2.13
NGC4372	5.07± 0.08	2.94± 0.14	0.16	0.23	0.42±0.02	28.59± 4.93
Rup106	19.94± 2.04	4.71± 0.67	0.14	0.38	0.76±0.04	46.00± 8.58
NGC4590	19.03± 1.44	8.86± 0.42	0.07	0.12	0.53±0.04	41.04± 8.30
NGC4833	4.09± 0.16	0.79± 0.12	0.17	0.51	0.81±0.03	44.23± 9.88
NGC5024	15.52± 0.92	9.09± 0.16	0.08	0.11	0.41±0.04	74.80± 1.44
NGC5053	13.99± 0.68	10.28± 0.09	0.29	0.36	0.26±0.04	76.11± 1.15
NGC5139	4.18± 0.03	1.35± 0.04	0.03	0.06	0.68±0.01	138.06± 0.89
NGC5272	10.29± 0.21	5.44± 0.09	0.05	0.08	0.47±0.01	56.37± 2.46
NGC5286	7.21± 0.45	1.16± 0.24	0.05	0.16	0.84±0.03	125.18±18.04
AM4	200.68±92.69	28.07± 2.24	0.17	0.65	0.86±0.07	83.67±10.52
NGC5466	36.74±13.50	7.95± 2.63	0.13	0.38	0.78±0.10	107.25± 2.20
NGC5634	14.09± 1.86	4.27± 2.30	0.08	0.17	0.70±0.14	64.17± 2.87
NGC5694	35.01± 3.92	3.98± 0.95	0.02	0.11	0.89±0.03	124.95± 8.69
IC4499	17.02± 1.83	6.38± 1.24	0.13	0.27	0.63±0.07	112.45± 1.86
NGC5824	26.72± 5.64	15.17± 5.45	0.03	0.04	0.43±0.18	57.22± 2.76
Pal5	20.90± 4.11	17.40± 6.04	0.55	0.63	0.17±0.20	65.13± 2.14
NGC5897	6.09± 0.87	2.86± 1.05	0.20	0.31	0.53±0.14	59.50±12.47
NGC5904	13.55± 0.53	2.90± 0.05	0.04	0.12	0.79±0.01	74.09± 0.66
NGC5927	4.70± 0.09	3.99± 0.02	0.10	0.12	0.15±0.02	9.13±20.45
NGC5946	3.33± 0.46	0.83± 0.43	0.09	0.22	0.75±0.12	77.17± 1.91
NGC5986	2.86± 0.28	0.67± 0.31	0.10	0.27	0.77±0.10	60.88±11.67
FSR1716	3.74± 0.31	2.55± 0.42	0.24	0.30	0.32±0.09	32.33±11.77
Pal14	49.36± 4.57	3.90± 1.90	0.29	1.70	0.92±0.04	75.06±193.30
Lynxa7	3.24± 0.26	1.91± 0.39	0.17	0.24	0.41±0.09	36.06± 9.71
NGC6093	1.93± 0.14	0.35± 0.10	0.08	0.28	0.82±0.05	97.02± 2.65
NGC6121	3.36± 0.06	0.55± 0.08	0.13	0.47	0.84±0.02	4.96± 7.66
NGC6101	29.13± 5.14	11.37± 1.07	0.10	0.20	0.61±0.07	143.36± 8.63
NGC6144	2.82± 0.30	2.27± 0.31	0.26	0.30	0.19±0.10	116.71± 3.09
NGC6139	2.43± 0.36	1.34± 0.45	0.07	0.10	0.45±0.15	62.30± 5.09
Ter3	2.76± 0.23	2.26± 0.11	0.36	0.40	0.18±0.07	42.91± 6.72
NGC6171	2.34± 0.09	1.02± 0.15	0.17	0.31	0.56±0.05	49.25± 6.55
ESO452-SC11	1.62± 0.19	0.48± 0.18	0.28	0.73	0.70±0.10	48.30± 1.71
NGC6205	4.94± 0.08	1.55± 0.04	0.07	0.15	0.69±0.01	105.00± 0.74
NGC6229	16.44± 1.73	1.94± 1.49	0.04	0.16	0.88±0.09	73.83±16.27
NGC6218	3.57± 0.06	2.35± 0.10	0.13	0.17	0.34±0.02	36.79± 4.40
FSR1735	3.13± 0.44	0.87± 0.27	0.27	0.65	0.72±0.08	67.41± 5.27
NGC6235	13.62± 9.74	5.43± 1.53	0.07	0.13	0.60±0.30	39.53± 2.06
NGC6254	3.28± 0.05	1.97± 0.04	0.12	0.16	0.40±0.01	42.78± 1.89
NGC6256	2.34± 0.32	2.13± 0.47	0.14	0.15	0.09±0.14	18.53± 8.09
Pal15	26.61± 2.86	1.68± 0.92	0.28	1.75	0.94±0.03	110.49±39.89
NGC6266	1.59± 0.06	0.83± 0.08	0.07	0.12	0.48±0.04	29.05± 6.51
NGC6273	2.28± 0.14	1.22± 0.11	0.09	0.14	0.46±0.05	99.61±12.71
NGC6284	4.32± 0.62	1.28± 0.39	0.09	0.20	0.70±0.09	90.47± 0.62

Table 1. *continued.*

ID	a (kpc)	R_{peri} (pc)	rh/r_{J_a}	$rh/r_{J_{R_{peri}}}$	ϵ	i (deg)
NGC6287	3.56± 0.80	1.25± 0.26	0.09	0.18	0.65±0.10	95.88± 0.50
NGC6293	1.76± 0.46	0.50± 0.18	0.23	0.61	0.72±0.11	130.42±54.17
NGC6304	2.39± 0.24	1.77± 0.23	0.19	0.23	0.26±0.09	19.66±31.83
NGC6316	3.12± 0.89	1.45± 0.87	0.09	0.15	0.54±0.24	34.75± 2.86
NGC6341	5.76± 0.12	1.00± 0.09	0.07	0.20	0.83±0.01	83.79± 1.45
NGC6325	1.35± 0.34	1.04± 0.13	0.11	0.13	0.23±0.20	106.50± 1.38
NGC6333	3.90± 0.39	1.16± 0.15	0.09	0.19	0.70±0.04	64.73± 3.63
NGC6342	1.50± 0.25	1.12± 0.34	0.12	0.15	0.25±0.17	62.88± 3.56
NGC6356	5.76± 1.16	3.17± 1.58	0.09	0.13	0.45±0.21	43.18± 2.20
NGC6355	1.50± 0.46	0.87± 0.24	0.15	0.22	0.42±0.20	103.08± 0.84
NGC6352	3.28± 0.30	2.98± 0.25	0.18	0.19	0.09±0.09	13.33±13.74
IC1257	10.03± 1.37	2.01± 0.72	0.36	0.99	0.80±0.07	158.42±31.57
Ter2	0.65± 0.23	0.18± 0.06	0.42	0.96	0.72±0.13	158.97±26.47
NGC6366	3.74± 0.10	2.04± 0.11	0.20	0.29	0.45±0.02	34.87± 4.76
Ter4	0.93± 0.29	0.41± 0.22	0.34	0.64	0.56±0.22	46.85± 2.07
HP1	1.24± 0.33	0.53± 0.23	0.27	0.54	0.57±0.18	87.68± 0.54
NGC6362	3.83± 0.05	2.52± 0.09	0.20	0.25	0.34±0.02	44.18± 3.07
Lil1	0.61± 0.16	0.14± 0.11	0.07	0.17	0.77±0.17	162.65±31.56
NGC6380	1.35± 0.37	0.33± 0.10	0.16	0.47	0.76±0.09	157.67±14.22
Ter1	0.86± 0.31	0.23± 0.17	0.23	0.60	0.73±0.19	13.39±11.30
Ton2	2.90± 0.44	2.02± 0.31	0.17	0.22	0.30±0.12	35.55± 3.74
NGC6388	2.45± 0.05	1.11± 0.02	0.06	0.11	0.55±0.01	154.64± 5.03
NGC6402	2.50± 0.13	0.65± 0.17	0.10	0.28	0.74±0.06	46.95± 5.07
NGC6401	1.32± 0.38	0.60± 0.41	0.14	0.27	0.55±0.26	51.33± 6.60
NGC6397	4.43± 0.02	2.63± 0.03	0.10	0.13	0.41±0.00	47.06± 0.42
Pal6	2.06± 0.37	0.40± 0.10	0.12	0.42	0.81±0.06	82.84± 0.78
NGC6426	121.07±83.20	26.84± 5.46	0.04	0.11	0.78±0.16	20.93± 4.24
Djor1	70.25±71.73	4.36± 1.76	0.03	0.20	0.94±0.07	6.00±17.61
Ter5	1.82± 0.31	0.82± 0.32	0.05	0.10	0.55±0.15	12.69±74.47
NGC6440	0.91± 0.19	0.30± 0.12	0.08	0.19	0.67±0.13	113.79± 2.79
NGC6441	2.45± 0.08	1.00± 0.08	0.05	0.10	0.59±0.03	20.82± 8.51
Ter6	0.92± 0.28	0.24± 0.09	0.15	0.41	0.74±0.12	157.28±21.98
NGC6453	2.91± 0.84	1.56± 0.90	0.16	0.23	0.46±0.26	78.02± 1.02
UKS1	0.65± 0.19	0.25± 0.22	0.32	0.63	0.62±0.29	11.86±37.46
NGC6496	7.78± 3.87	4.02± 0.94	0.17	0.26	0.48±0.27	30.99± 5.88
Ter9	0.73± 0.24	0.18± 0.09	0.92	2.29	0.75±0.14	69.96± 2.58
Djor2	1.83± 0.46	0.82± 0.37	0.17	0.32	0.55±0.19	11.51± 6.50
NGC6517	2.37± 0.37	0.50± 0.15	0.07	0.21	0.79±0.07	58.10± 5.92
NGC6522	0.68± 0.17	0.28± 0.20	0.47	0.89	0.59±0.25	71.88±123.80
Ter10	1.68± 0.29	0.94± 0.23	0.26	0.41	0.44±0.13	58.94± 0.74
NGC6535	2.74± 0.16	1.01± 0.23	0.29	0.58	0.63±0.07	161.39±27.30
NGC6528	1.01± 0.44	0.41± 0.10	0.21	0.43	0.59±0.19	65.60± 1.95
NGC6539	2.66± 0.13	1.98± 0.16	0.17	0.20	0.26±0.05	56.14± 5.48
NGC6540	2.12± 0.31	1.43± 0.37	0.21	0.28	0.33±0.14	22.44± 1.48
NGC6544	3.05± 0.19	0.62± 0.20	0.11	0.33	0.80±0.06	66.51± 1.67
NGC6541	2.70± 0.14	1.76± 0.21	0.10	0.14	0.35±0.06	46.22± 4.45
ESO280-SC06	9.75± 1.45	3.35± 1.77	0.28	0.55	0.66±0.16	61.52± 3.56
NGC6553	1.82± 0.15	1.29± 0.22	0.13	0.17	0.29±0.09	13.70±50.10
2MASS-GC02	1.46± 0.27	0.48± 0.22	0.32	0.77	0.67±0.14	170.20±78.55
NGC6558	1.17± 0.42	0.58± 0.10	0.24	0.42	0.50±0.19	62.45±22.78
IC1276	4.61± 0.31	3.47± 0.12	0.17	0.21	0.25±0.05	10.88±43.39
Ter12	4.41± 0.26	2.99± 0.26	0.12	0.15	0.32±0.05	18.98± 1.82
NGC6569	2.39± 0.63	1.84± 0.92	0.12	0.14	0.23±0.27	26.98±47.90
BH261	1.94± 0.36	1.30± 0.55	0.13	0.17	0.33±0.20	34.28± 0.83
NGC6584	10.68± 3.70	2.10± 1.08	0.08	0.24	0.80±0.11	52.19± 3.19
NGC6624	1.01± 0.09	0.46± 0.14	0.15	0.28	0.54±0.11	68.41± 7.54
NGC6626	1.74± 0.13	0.57± 0.10	0.09	0.20	0.67±0.05	60.27± 3.62
NGC6638	1.67± 0.45	0.40± 0.13	0.11	0.34	0.76±0.09	77.99± 3.32
NGC6637	1.40± 0.32	0.73± 0.54	0.16	0.26	0.48±0.29	74.26± 1.27
NGC6642	1.24± 0.16	0.37± 0.15	0.17	0.45	0.70±0.11	62.26± 8.94
NGC6652	2.15± 0.54	0.65± 0.49	0.09	0.22	0.70±0.20	74.62± 0.91
NGC6656	6.20± 0.03	2.96± 0.05	0.07	0.11	0.52±0.01	33.66± 1.91
Pal8	4.01± 0.74	2.44± 1.11	0.28	0.38	0.39±0.21	22.17± 5.51
NGC6681	2.91± 0.15	0.84± 0.08	0.10	0.23	0.71±0.03	91.13± 3.71

Table 1. *continued.*

ID	a (kpc)	R_{peri} (pc)	rh/r_{J_a}	$rh/r_{J_{R_{peri}}}$	ϵ	i (deg)
NGC6712	2.61± 0.07	0.45± 0.10	0.16	0.57	0.83±0.04	83.31± 6.76
NGC6715	24.76± 1.08	12.58± 0.47	0.02	0.03	0.49±0.03	83.60± 0.55
NGC6717	1.81± 0.15	0.89± 0.17	0.35	0.60	0.51±0.08	34.60± 6.62
NGC6723	2.46± 0.08	2.08± 0.14	0.16	0.17	0.15±0.03	86.46± 9.56
NGC6749	3.34± 0.19	1.60± 0.28	0.21	0.33	0.52±0.07	3.59±122.04
NGC6752	4.30± 0.04	3.23± 0.08	0.08	0.10	0.25±0.01	25.96± 2.85
NGC6760	3.79± 0.11	1.90± 0.09	0.10	0.15	0.50±0.02	6.80±75.96
NGC6779	6.68± 0.43	0.97± 0.38	0.10	0.34	0.85±0.05	106.58± 8.68
Ter7	28.93± 9.38	13.14± 2.68	0.13	0.22	0.55±0.16	84.81± 0.64
Pal10	5.52± 0.21	4.01± 0.31	0.10	0.12	0.27±0.04	7.62±40.80
Arp2	39.67±10.04	18.46± 3.05	0.15	0.27	0.53±0.13	76.93± 1.25
NGC6809	3.57± 0.08	1.59± 0.02	0.17	0.27	0.55±0.01	67.31± 1.06
Ter8	35.05±10.66	16.23± 3.06	0.15	0.27	0.54±0.15	82.98± 0.80
Pal11	7.30± 1.21	5.43± 2.07	0.22	0.27	0.26±0.19	26.14±11.54
NGC6838	5.93± 0.03	4.77± 0.06	0.15	0.18	0.19±0.01	11.87±11.19
NGC6864	10.02± 1.50	2.06± 1.15	0.03	0.08	0.79±0.11	49.76± 8.30
NGC6934	21.06± 5.32	2.60± 1.12	0.04	0.16	0.88±0.06	23.41±46.62
NGC6981	12.65± 2.29	1.29± 0.74	0.09	0.41	0.90±0.06	67.90±35.70
NGC7006	28.76± 2.84	2.07± 0.94	0.06	0.34	0.93±0.03	135.42±28.56
NGC7078	6.98± 0.05	3.57± 0.06	0.04	0.06	0.49±0.01	28.59± 1.69
NGC7089	8.68± 0.30	0.56± 0.10	0.04	0.27	0.94±0.01	84.10±28.49
NGC7099	4.82± 0.25	1.49± 0.05	0.11	0.23	0.69±0.02	118.50± 6.29
Pal12	43.46±18.94	15.75± 1.92	0.14	0.28	0.64±0.16	67.35± 3.08
Pal13	38.26± 5.50	9.04± 1.74	0.26	0.74	0.76±0.05	112.26± 6.36
NGC7492	16.25± 1.88	4.27± 2.29	0.18	0.45	0.74±0.12	91.70± 1.20